Kinematic Characteristics and Risk Analysis of Potential Rockfall based on 3D Point Clouds

Wei Yuan[1], Changqing Liu[1,2], Han Bao[2], Weihang Ran[4],
Zhongyuan Yang[1], Xiuxiao Yuan[3], Ryosuke Shibasaki[4], Shunichi Koshimura[1]

[1] Tohoku University, Sendai, Japan
[2] Chang’an University, Xi’an, China
[3] Wuhan University, Wuhan, China
[4] The University of Tokyo, Tokyo, Japan

Keywords: 3D point cloud, kinematic analysis, rockfall source identification, rock characterisation, rockfall trajectory

Abstract

Rockfall hazard on steep rock slopes is strongly controlled by the geometry of in-situ blocks bounded by intersecting discontinuities. In practice, however, source blocks are still commonly identified by field observation and manual interpretation, which is difficult to apply consistently on high, steep slopes. This study develops a three-dimensional point-cloud-based workflow for locating, characterising, and assessing potentially unstable rock blocks under real terrain conditions. The approach combines structural interpretation with visual kinematic criteria to detect discontinuity combinations associated with planar sliding, wedge sliding, and toppling, and to map unstable blocks directly in point-cloud space. Block volumes are then estimated by point-cloud differencing, allowing the number and size distribution of source blocks to be described quantitatively. Finally, representative blocks are introduced into three-dimensional rockfall simulations using their measured location and volume. The simulations provide rockfall frequency, bounce height, velocity, and kinetic energy, and are used to evaluate the threat posed to the transportation corridor below the slope. The proposed workflow links source identification with dynamic hazard assessment and offers a practical basis for rapid screening and refined mitigation of rockfall-prone slopes in mountainous infrastructure corridors.

Figure 1. Representative potentially unstable rock block formed by intersecting discontinuities above the roadway.

1. Introduction

Potentially unstable rock blocks are closed rock masses bounded by intersecting discontinuities in fractured slopes (Li et al., 2025; Ren et al., 2025). Their shape, size, and position influence not only whether failure can occur, but also how detached blocks are likely to move and what they may strike downslope (Bao et al., 2025; Wang et al., 2025). This makes block identification a necessary starting point for both stability analysis and rockfall mitigation design along steep transportation corridors (Ma et al., 2022; Liu et al., 2024). The difficulty is that on high and irregular slopes these blocks are often partly concealed, their boundaries are hard to trace, and their consequences can be severe once released. As a result, the source area is usually the least certain part of the hazard chain. Figure 1 shows a representative source block exposed above the roadway.

For a long time, unstable rock blocks have mainly been identified through field mapping, manual interpretation, and expert judgement. These approaches may be workable for small engineering sites, but they are difficult to apply efficiently to high and steep rock slopes, where terrain occlusion, limited visibility, operational risk, and interpretative subjectivity restrict the rapid and quantitative characterisation of block boundaries, volume, and spatial distribution (Wu et al., 2021). Recent advances in terrestrial laser scanning, UAV photogrammetry, and dense image matching techniques have made it possible to obtain high-resolution, non-contact, and large-area geometric information from rock-slope surfaces (Yuan et al., 2023; Liu et al., 2026a; Yuan et al., 2025). As a result, point-cloud-based structural analysis and unstable block identification have become active topics in engineering geology and rock engineering. Point clouds preserve the surface morphology of slopes and the exposure geometry of discontinuities with high fidelity, thereby supporting discontinuity orientation extraction, spatial relationship analysis, and block reconstruction. This development has promoted a shift from experience-based interpretation towards three-dimensional quantitative analysis (Chen et al., 2016; Jiang et al., 2020).

Rockfall dynamics form the second key component of hazard assessment once an unstable block is detached. After release, rockfall motion is typically nonlinear and strongly affected by slope topography, surface cover, block shape and size, release position, and rebound behaviour. A large body of previous work has addressed these processes through theoretical analysis (Asteriou and Tsiambaos, 2016), laboratory experiments (Lambert et al., 2020), field monitoring (Gili et al., 2022), and numerical simulation (He et al., 2017). Theoretical models help clarify the governing mechanics, but usually require simplified assumptions about block geometry, boundary conditions, and impact processes, which limits their applicability on natural slopes. Laboratory experiments provide controlled observations of impact, rebound, and energy dissipation, yet scale effects and material similarity constraints complicate transfer to real slopes. Field monitoring captures more realistic behaviour, but

https://doi.org/10.5194/isprs-archives-XLIX-B4-2026-223-2026

remains difficult to conduct on steep rock slopes because of cost, safety, and logistical constraints (Ma et al., 2021). Numerical simulation has therefore become a widely used tool because it is efficient, repeatable, and well suited to visualising rockfall processes and risk patterns.

This study addresses that gap by treating source identification and post-failure motion as parts of the same problem. The spatial relationship between discontinuities and slope morphology is first used to identify structural combinations capable of producing instability. The resulting in-situ block positions and volumes are then transferred to three-dimensional rockfall simulations so that source conditions and runout behaviour remain physically linked. The aim is to build a practical workflow that starts with block localisation and ends with hazard assessment, and that can support screening, zoning, and mitigation for steep mountain slopes above transportation infrastructure.

2. Related Work

Research on unstable rock-block identification and characterisation from point-cloud data has developed from basic slope reconstruction towards discontinuity extraction, intersection inference, block closure analysis, and volume estimation. Previous studies have shown that discontinuity normals and spatial geometric relationships can be used effectively to identify the key structural surfaces controlling block formation, offering a practical route for in-situ block detection (Cheng et al., 2024). For example, Chen et al. (2016) combined terrestrial laser-scanning point clouds with discontinuity intersection geometry to construct candidate blocks, and then extracted real blocks automatically through spatial filtering and volume calculation. Three-dimensional models derived from UAV imagery have also been applied to the quantitative estimation of unstable block volume in engineering practice. By extracting potential rupture surfaces and spatially cutting target blocks, such studies have enabled quantitative description of block geometry under real slope conditions (Wang et al., 2018; Fu et al., 2024; Yuan et al., 2025). Overall, point-cloud and realistic three-dimensional reconstruction techniques have improved the objectivity and resolution of unstable block surveys, but most existing studies still focus on block extraction and volume estimation themselves. Less attention has been given to how such identification results can be used directly in failure-mode interpretation and rockfall risk analysis.

At the same time, rockfall simulation has evolved from simplified two-dimensional approaches to more detailed three-dimensional analysis as computing power and terrain modelling techniques have advanced. Existing models can be broadly grouped into lumped-mass models, hybrid models, and rigid-body dynamic models, each with different strengths in computational efficiency, process representation, and sensitivity to block shape (Dorren, 2003; Volkwein et al., 2011). LiDAR- and GIS-based spatial modelling has also been used to connect terrain representation with rockfall hazard analysis (Lan et al., 2010). In recent years, platforms such as Rockfall Analyst, RocPro3D, and RAMMS::Rockfall have matured and shown clear advantages for trajectory simulation, bounce-height estimation, velocity evolution, and kinetic-energy prediction under real terrain conditions. These tools are now widely used in rockfall hazard assessment and mitigation design along mountain roads, railways, and other critical infrastructure (Lan et al., 2007; Wu et al., 2025). Even so, the realism of numerical simulation still depends strongly on how the source area is defined. In many studies, release points are still selected empirically or simplified in ways that do not fully represent the true in-situ location and geometry of unstable blocks. This weakens the link between simulated motion and actual hazard development.

For steep rock slopes, unstable block identification and rockfall dynamics should be treated as consecutive and mutually supporting steps. If the in-situ position, volume, and structural controls of unstable blocks are not characterised adequately, the source parameters used in subsequent simulation are unlikely to be reliable. Conversely, if unstable block identification remains limited to geometric description without being linked to likely failure modes and post-failure motion, its value for engineering hazard mitigation remains incomplete. There is therefore a clear need for an integrated analytical framework in which high-resolution three-dimensional terrain reconstruction supports block identification, geometric characterisation, and rockfall simulation in a consistent manner. Such a framework can improve the realism, relevance, and engineering usefulness of rockfall hazard assessment in complex terrain.

3. Methods

The workflow combines structural interpretation, geometric characterisation, and dynamic simulation within the same terrain model. It begins with the extraction of discontinuity geometry from the three-dimensional point cloud, including the location, orientation, and geometric extent of the main structural surfaces (Liu et al., 2026a). These data are then evaluated with the ROKA method proposed by Menegoni et al. (2021), which tests potential failure modes against locally variable slope geometry. Because the method accounts for changes in slope aspect, dip, and discontinuity combinations, it is suitable for identifying planar sliding, wedge sliding, and toppling conditions on complex rock slopes. In effect, this step converts discontinuity geometry into explicit kinematic constraints and narrows the search space for unstable blocks.

Once candidate source blocks have been delimited, their geometry is quantified with the “Compute 2.5D Volume” tool in CloudCompare. The study area is subdivided into regular grid cells matched to the point-cloud resolution. For each cell, the elevation difference between the rock surface and the assumed basal surface is calculated. Integrating the elevation difference H_i over all cells of size D_i gives the block volume $V_{2.5D}$ according to Eq. 1. The result is a set of unstable blocks with mapped position and estimated volume, which can then be grouped by size for subsequent interpretation.

$$V_{2.5D} = \sum_i D_i^2 \cdot H_i \tag{1}$$

where $V_{2.5D}$ is the estimated block volume, D_i is the grid-cell size, and H_i is the elevation difference in the ith cell.

The final stage uses these mapped source blocks in three-dimensional rockfall simulations carried out in Rockfall Analyst. A digital elevation model derived from the point-cloud data is used to represent the slope surface, while the in-situ block locations define the release points. Block volume and geometry are translated into model input parameters, including the initial coordinates (x_0, y_0, z_0) and initial velocity components (v_{x0}, v_{y0}, v_{z0}). The simulation workflow is summarized in Figure 2.

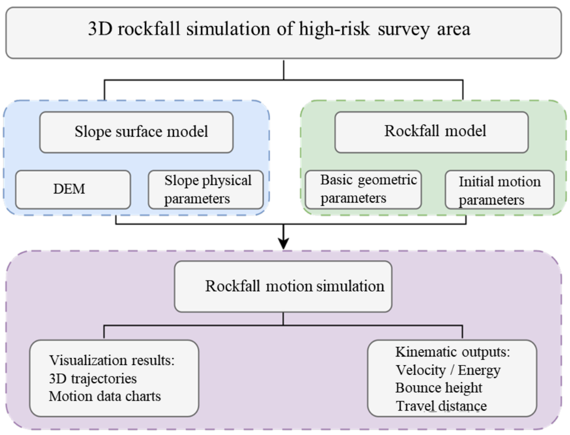

Figure 2. Workflow for rockfall motion simulation using Rockfall Analyst.

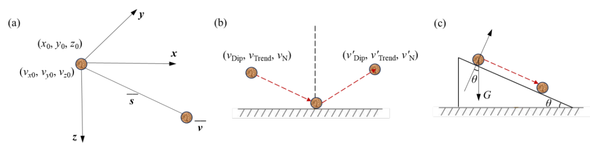

Figure 3. Schematic illustration of rockfall motion stages: (a) free fall, (b) impact-rebound, and (c) rolling-sliding.

The main motion stages represented in the model are illustrated in Figure 3. The simulation accounts for free fall, rebound, rolling, and sliding, and repeated stochastic runs are used to describe the distribution of trajectory, frequency, bounce height, velocity, and kinetic energy. These outputs are then interpreted in terms of potential impact on the transportation structures below the slope.

4. Results and Analysis

4.1 Identification of Potentially Unstable Rock Blocks Using the ROKA Method

The ROKA analysis was applied to the discontinuity sets extracted from the high-resolution point-cloud model in order to screen the slope for kinematically feasible failures. For planar sliding and toppling controlled by a single discontinuity set, each structural plane was represented as a disc with a defined orientation and extent, and the irregular point-cloud-derived slope surface was treated as the free face. Potential block boundaries were identified from the spatial intersection between these elements. For wedge sliding, the analysis considered blocks formed by paired discontinuity sets and tested whether the line of intersection, together with the local slope geometry, permitted movement either along the intersection line or along one of the controlling planes. Because the procedure evaluates local slope aspect, dip angle, and surface curvature, it is able to screen for unstable blocks under strongly variable terrain conditions. Details of the full identification procedure are given by Liu et al. (2026b).

In total, 102 potentially unstable rock blocks were identified within the study area, indicating strong block development under the control of intersecting discontinuities on this steep rock slope. The number of blocks varied substantially among the survey zones. SA3 contained the largest number, with 16 identified blocks, whereas SA5 contained the fewest, with 7. This variation indicates that block occurrence is not random but jointly controlled by local structural combinations, slope geometry, and free-face development.

4.2 Volume Characterisation and Spatial Distribution of Unstable Rock Blocks

After the kinematically admissible blocks had been delineated, their geometry was quantified by block extraction and volume estimation in each survey zone. Estimated block volume ranged from 0.219 to 9.062 m^3. The range is broad enough to show that the slope contains both small localised source blocks and much larger blocks with greater destructive potential. It also reflects the uneven spatial development of discontinuity combinations, block partitioning, and free-face exposure across the slope.

To describe regional differences in block size composition, the classification proposed by Calio et al. (2023) was adopted. In-situ unstable blocks were divided into four classes: small (< 0.5 m^3), medium (0.5–1 m^3), large (1–2.5 m^3), and extra-large (> 2.5 m^3). The statistical results show that large blocks dominate most source zones and represent the most common volume class in the study area. Figure 4 summarizes the volume-class composition across all survey zones.

Large blocks accounted for 41.7%, 42.9%, and 40.1% of the total in SA1, SA2, and SA6, respectively. In these three zones, extra-large blocks formed the second most common class, ranging from 25.0% to 33.3%, whereas small blocks represented only 7.1% to 13.3%. In SA3 and SA8, the dominance of the large class was even more pronounced, accounting for 50.0% and 55.6%, respectively, which indicates a relatively concentrated size distribution. SA5 showed a different pattern, with medium and large blocks each accounting for 42.9%, while extra-large blocks represented only 14.3%. SA7 displayed the simplest size structure: 62.5% of the unstable blocks fell within the large class and 37.5% within the extra-large class, with no small or medium blocks identified. This indicates that SA7 is the zone with the greatest concentration of large and extra-large unstable blocks on the slope. SA4 and SA9 exhibited more balanced distributions between the medium and large classes. In SA4, medium and large blocks accounted for 33.3% and 44.4%, respectively, whereas in SA9 the corresponding values were 41.7% and 33.3%.

Taken together, these results show that block-size composition varies markedly from one source zone to another. That variation matters for hazard management because it affects both the likely number of released blocks and the expected scale of impact. The volume statistics therefore provide a practical basis for distinguishing zones that require different levels of protection or different mitigation priorities.

4.3 Rockfall Dynamic Response Simulated with Rockfall Analyst

Source zone SA2 was selected for detailed simulation because it provides a representative case in which multiple unstable blocks are concentrated above the transportation corridor. The unstable blocks mapped in this zone were used as release sources in Rockfall Analyst. Each block was released from its in-situ position, and the measured volume was converted to a corresponding mass input. Because rockfall motion is not deterministic, 50 particles with the same mass were released from each source point so that

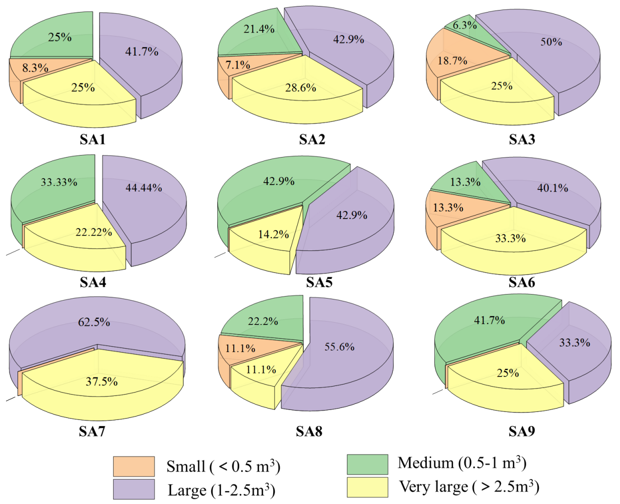

Figure 4. Three-dimensional fan chart illustrating the volumetric classification of unstable rock blocks across survey zones SA1–SA9 on the steep rock slope.

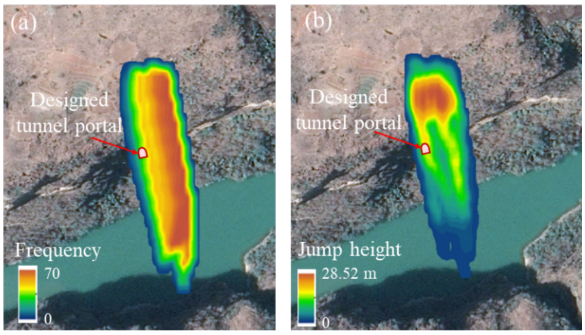

Figure 5. Spatial distribution of simulated rockfall dynamic parameters for source zone SA2: (a) rockfall frequency and (b) bounce height.

the resulting trajectory pattern and dynamic indicators could be interpreted statistically rather than from a single path.

The SA2 simulations do not produce an even spread of trajectories. Instead, the paths concentrate strongly in specific parts of the slope, which indicates that local topography exerts a clear steering effect on rockfall propagation. The simulated spatial distribution of the dynamic parameters is shown in Figure 5. The highest trajectory frequency occurs on the right-hand side of the pathway, where the maximum count reaches 70. Even after repeated impacts and deflections, many trajectories continue to converge into the same grooves or along the dominant downslope direction. Bounce height shows a similarly uneven pattern. The highest values occur in the upper part of the path and approach 28 m, which is consistent with the steep source area and the rapid conversion of potential energy immediately after release. In practical terms, the upper slope segment is the part of the path where vertical motion is developed most strongly.

To look more closely at the behaviour of a single source block, block SA2-8 was selected because its simulated path passes near the tunnel portal. A representative slope profile was extracted along that path, and the trajectory and velocity history were examined in detail (Figure 6). The dynamic response is distinctly non-stationary: both velocity and bouncing vary in a saw-tooth

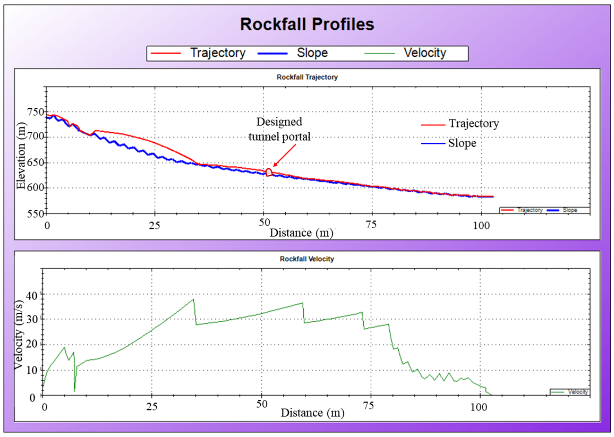

Figure 6. Trajectory profile and velocity history of representative block SA2-8 along a rockfall path intersecting the tunnel portal.

pattern with travel distance rather than following a smooth trend. This behaviour suggests repeated disturbance by small-scale topographic relief, local scarps, and rough structural surfaces, so that the block alternates frequently between rolling contact and short airborne phases. The maximum simulated velocity reaches 38 m/s. High bounce values are concentrated near slope breaks, local protrusions, or points where high-speed impact leads to renewed projection, whereas velocity peaks appear where potential energy is converted rapidly and terrain guidance is strong.

5. Conclusion

This study presents a workflow that keeps source identification and rockfall simulation within the same analytical framework. The results show that kinematically admissible unstable blocks can be located directly from point-cloud-derived structural information, and that large blocks form the dominant volume class in most source zones of the study slope. When the in-situ position and volume of these blocks are transferred to three-dimensional rockfall simulation, the analysis yields a more explicit description of where hazardous blocks are located, how frequently they may reach particular paths, and what level of impact energy they may retain near critical infrastructure. In that sense, the main contribution of the study is not a single algorithmic step, but the integration of block localisation, volume estimation, and dynamic hazard assessment into one practical workflow. This makes the approach suitable for rapid screening and for more detailed mitigation planning on steep rock slopes along mountain transportation corridors.

Acknowledgements

This work is supported by the JSPS Kakenhi (Grants-in-Aid for Scientific Research 23K13419), the Co-Creation Center for Disaster Resilience, Tohoku University, and the Cross-Ministerial Strategic Innovation Promotion Program (Grant Number JPJ012289).

References

Asteriou, P., Tsiambaos, G., 2016: Empirical model for predicting rockfall trajectory direction. *Rock Mechanics and Rock Engineering*, 49(3), 927–941. doi: 10.1007/s00603-015-0798-7.

Bao, H., Li, X.G., Liu, L., Song, Z.T., Lan, H.X., Yan, C.G., Jiang, Z.Y., 2025: Research progress on disaster mechanisms and lightweight monitoring and early warning of highway slopes. *China Journal of Highway and Transport*, 38(10), 1–20. doi: 10.19721/j.cnki.1001-7372.2025.10.001.

Calio, D., Mineo, S., Pappalardo, G., 2023: Digital Rock Mass Analysis for the Evaluation of Rockfall Magnitude at Poorly Accessible Cliffs. *Remote Sensing*, 15(6).

Chen, J., Zhu, H., Li, X., 2016: Automatic extraction of discontinuity orientation from rock mass surface 3D point cloud. *Computers and Geosciences*, 95, 18–31. doi: 10.1016/j.cageo.2016.06.015.

Cheng, Y., Li, Y., Xia, J., Hou, Z., Chen, N., 2024: Application of UAV technology to the semi-automatic identification of dangerous rock masses on ultra-high steep slopes. *The Chinese Journal of Geological Hazard and Control*, 35(1), 143–154. doi: 10.16031/j.cnki.issn.1003-8035.202310028.

Dorren, L.K.A., 2003: A review of rockfall mechanics and modelling approaches. *Progress in Physical Geography*, 27(1), 69–87. doi: 10.1191/0309133303pp359ra.

Fu, D., Wang, S., Wu, B., Xia, X., 2024: Construction and analysis of high-steep slope unstable rock features based on UAV photogrammetry. *Acta Geoscientica Sinica*, 45(1), 53–62. doi: 10.3975/cagsb.2023.030202.

Gili, J.A., Ruiz-Carulla, R., Matas, G., Moya, J., Prades, A., Corominas, J., Lantada, N., Nunez-Andres, M.A., Buill, F., Puig, C., 2022: Rockfalls: analysis of the block fragmentation through field experiments. *Landslides*, 19, 1009–1029. doi: 10.1007/s10346-021-01837-9.

He, P., Li, S., Li, L., Zhang, Q., Xu, F., Chen, Y., 2017: Discontinuous deformation analysis of super section tunnel surrounding rock stability based on joint distribution simulation. *Computers and Geotechnics*, 91, 218–229. doi: 10.1016/j.compgeo.2017.07.022.

Jiang, N., Li, H.B., Liu, M.S., Zhang, J.Y., Zhou, J.W., 2020: Quantitative hazard assessment of rockfall and optimization strategy for protection systems of the Huashiya cliff, southwest China. *Geomatics, Natural Hazards and Risk*, 11(1), 1939–1965. doi: 10.1080/19475705.2020.1819445.

Lambert, S., Bourrier, F., Gotteland, P., Nicot, F., 2020: An experimental investigation of the response of slender protective structures to rockfall impacts. *Canadian Geotechnical Journal*, 57(8), 1215–1231. doi: 10.1139/cgj-2019-0147.

Lan, H., Martin, C.D., Lim, C.H., 2007: RockFall Analyst: A GIS extension for three-dimensional and spatially distributed rockfall hazard modeling. *Computers and Geosciences*, 33(2), 262–279. doi: 10.1016/j.cageo.2006.05.013.

Lan, H., Martin, C.D., Zhou, C., Lim, C.H., 2010: Rockfall hazard analysis using LiDAR and spatial modeling. *Geomorphology*, 118(1–2), 213–223. doi: 10.1016/j.geomorph.2010.01.002.

Li, Z., Ji, F., Zeng, R., Lu, Y., Ding, J., Wu, C., 2025: Deformation and failure mechanisms of weak-based columnar rock masses characterized by physical simulation. *Engineering Failure Analysis*, 185, 110418. doi: 10.1016/j.engfailanal.2025.110418.

Liu, C.Q., Bao, H., Lan, H.X., Yan, C.G., Li, C.B., Liu, S.J., 2024: Failure evaluation and control factor analysis of slope block instability along traffic corridor in Southeastern Tibet. *Journal of Mountain Science*, 21(6), 1830–1848. doi: 10.1007/s11629-023-8484-9.

Liu, C.Q., Bao, H., Wang, T.Y., Zhang, J.F., Lan, H.X., Qi, S.W., Yuan, W., Koshimura, S., 2026a: Intelligent characterization of discontinuities and heterogeneity evaluation of potential hazard sources in high-steep rock slope by TLS-UAV technology. *Journal of Rock Mechanics and Geotechnical Engineering*, 18(1), 509–527. doi: 10.1016/j.jrmge.2025.03.023.

Liu, C.Q., Bao, H., Zhang, J.F., Yang, J.H., Dong, X.Y., Lan, H.X., Koshimura, S., Yuan, W., 2026b: Quantitative identification and hazard assessment of potentially unstable rock masses along mountainous transportation corridors. *Engineering Failure Analysis*, 183, 110273. doi: 10.1016/j.engfailanal.2025.110273.

Ma, K., Liu, G., Xu, N., Zhang, Z., Feng, B., 2021: Motion characteristics of rockfall by combining field experiments and 3D discontinuous deformation analysis. *International Journal of Rock Mechanics and Mining Sciences*, 138, 104591. doi: 10.1016/j.ijrmms.2020.104591.

Ma, K., Liu, G.Y., 2022: Three-Dimensional discontinuous deformation analysis of failure mechanisms and movement characteristics of slope rockfalls. *Rock Mechanics and Rock Engineering*, 55(1), 275–296. doi: 10.1007/s00603-021-02656-z.

Menegoni, N., Giordan, D., Perotti, C., 2021: An open-source algorithm for 3D rock slope kinematic analysis (ROKA). *Applied Sciences*, 11(4), 1698. doi: 10.3390/app11041698.

Ren, M., Ding, Y., Hu, J., Wang, W., Ma, G., He, M., 2025: Automatic characterization of rock blocks in jointed exposures using 3D point clouds. *Engineering Geology*, 362, 108522. doi: 10.1016/j.enggeo.2025.108522.

Volkwein, A., Schellenberg, K., Labiouse, V., Agliardi, F., Berger, F., Bourrier, F., Dorren, L.K.A., Gerber, W., Jaboyedoff, M., 2011: Rockfall characterisation and structural protection - a review. *Natural Hazards and Earth System Sciences*, 11, 2617–2651. doi: 10.5194/nhess-11-2617-2011.

Wang, D., Zou, Y., Zhang, G., Hou, W., Deng, H., 2018: Application of photographic technique by unmanned aerial vehicle to dangerous rock exploration. *Journal of Chengdu University of Technology (Science & Technology Edition)*, 45(6), 754–759. doi: 10.3969/j.issn.1671-9727.2018.06.11.

Wang, J., Zheng, J., Hu, J., Jimenez, R., Zhu, A., Lu, Q., Wang, J., 2025: In-situ block intelligent identification: large-scale artificial intelligence models enable efficient geological surveys via image segmentation. *Engineering Geology*, 356, 108286. doi: 10.1016/j.enggeo.2025.108286.

Wu, F.Q., Wu, J., Bao, H., Li, B., Shan, Z.G., Kong, D.H., 2021: Advances in statistical mechanics of rock masses and its engineering applications. *Journal of Rock Mechanics and Geotechnical Engineering*, 13(1), 22–45. doi: 10.1016/j.jrmge.2020.11.003.

Wu, M., Luo, G., Hu, X., Bi, Y., Wang, Y., Ma, N., 2025: Dynamic fragmentation analysis of potential rockfall hazards at Zixia hydropower dam, Qinghai-Tibet Plateau. *Journal of Rock Mechanics and Geotechnical Engineering*, 17(7), 4109–4123. doi: 10.1016/j.jrmge.2024.12.005.

Yuan, W., Liu, C., Wang, T., Adriano, B., Bao, H., Shibasaki, R., Koshimura, S., 2025: Multi-source 3D point clouds fusion for potential rock mass hazard evaluation in high-steep rock slopes. *The International Archives of the Photogrammetry, Remote Sensing and Spatial Information Sciences*, XLVIII-G-2025, 1663–1668. doi: 10.5194/isprs-archives-XLVIII-G-2025-1663-2025.

Yuan, W., Yuan, X., Cai, Y., Shibasaki, R., 2023: Fully automatic DOM generation method based on optical flow field dense image matching. *Geo-spatial Information Science*, 26(2), 242–256. doi: 10.1080/10095020.2022.2159886.